

Effects of High-Temperature Characteristics of Calcium Ferrites on the Sinter Strength



LEONARDO TOMAS DA ROCHA, SEONGKYU CHO, SUNG-WAN KIM,
and SUNG-MO JUNG

Iron ore sinter is the main burden charged into the blast furnace. The liquid phase formed during the sintering process plays an important role in the agglomeration process, which affects the quality of the final product. The current study aims to clarify the effect of iron ores on the high-temperature characteristics of calcium ferrites (CFs). It was attempted to use two of the most common iron ores being used in the steel companies worldwide as the raw materials to prepare three kinds of CFs. The gangue components (SiO_2 , Al_2O_3) in the iron ores significantly affected the high-temperature characteristics of CF. By changing the CF used to assimilate with the sinter mix, the phases formed in the assimilated region were not significantly modified. For all the CFs, 'SFCA-related' phases were found to exist, which is believed that the sinter mix played the main role in the phase formation. Among several high-temperature characteristics, a melt index was newly suggested where its linear relationship coefficient with the penetration length of CFs was calculated to be 0.863. CFs containing a significant amount of gangue showed a low fluidity index and high dissolution of sinter mix, which resulted in the decrease in melt index. This CF consequently had low penetration depth into the sinter mix, which might jeopardize the agglomeration process of the sinter mix. The addition of all kinds of CFs to the standard sinter mix improved the compressive strength of the sinter. However, the strengthening behavior depends on the type and amount of CF.

<https://doi.org/10.1007/s11663-022-02612-4>

© The Minerals, Metals & Materials Society and ASM International 2022

I. INTRODUCTION

IRON ore sinter is the main iron-bearing material being used in the blast furnace (BF).^[1–5] During the sintering process of iron ores, the formation and flow of the liquid phase play very important roles in the agglomeration process of the particles, which are directly related to the quality of sintered ore.^[2,6] The sinter quality which is mainly represented by the strength, reducibility, and reduction disintegration is closely affected by the bonding phases formed during the sintering process.^[5–8] The characteristics of original iron ores used in the sintering process are one of the important parameters affecting the formation of

bonding phases,^[3,9–12] as the iron ores mined around the world have a wide range of chemical composition and structure.^[12]

The selection criteria for iron ores in the sintering process have been considered to be mostly the chemical composition,^[3,10,13] which means that iron ores containing a high amount of total Fe and low amount of gangue components such as SiO_2 and Al_2O_3 would be regarded as the high-grade materials for the sintering process. However, during the sintering process, the sinter mix containing iron ores is exposed to temperatures above $1300\text{ }^\circ\text{C}$ ^[14] and the behavior of the constituents of the sinter mix at high temperatures might be the essential factor for selecting the proper iron ore.^[13,15] Several researches showed that the high-temperature characteristics such as fluidity and assimilation behavior are dependent on the type of iron ore,^[10,15,16] which might change the characteristics of calcium ferrite according to the blend of ores used in the sinter mix, and consequently affect the properties of sinter such as yield and strength. Wu *et al.*^[15] correlated the shatter index of sinter with the fluidity of the blend of ores and showed that the relationship is not directly proportional. The fluidity index improves the shatter index up to an optimum value, followed by deterioration.

LEONARDO TOMAS DA ROCHA, SEONGKYU CHO, and SUNG-MO JUNG are with the Graduate Institute of Ferrous Technology (GIFT), Pohang University of Science and Technology (POSTECH), Pohang 37673, Korea. Contact e-mail: smjung@postech.ac.kr SUNG-WAN KIM is with the Ironmaking & FINEX Research Group, Process and Engineering Research Lab., POSCO, Pohang 37763, Korea.

Manuscript submitted March 28, 2022; accepted July 21, 2022.

Article published online August 12, 2022.

Previous studies investigated the interaction between reagent-grade calcium ferrite and several kinds of iron ores.^[5,17,18] All the aforementioned researches studied the penetration behavior of reagent-grade calcium ferrite into the iron ore substrate. In the case of Nakashima *et al.*,^[2] the substrate was replaced with reagent-grade hematite. The penetration length of the calcium ferrite was affected by the chemical composition of iron ores. As the Al₂O₃ content in iron ores increased, the penetration of reagent-grade calcium ferrite has deteriorated.^[5,17,18] Okazaki *et al.*^[17] also showed that an increase in the SiO₂ and the combined water level would also decrease the length of penetration achieved by the melt. Such a phenomenon would be resulted because those components modify the viscosity of the melt and the surface structure of iron ore, respectively. Okazaki *et al.*^[17] and Nakashima *et al.*^[2] also correlated the penetration behavior of the reagent-grade calcium ferrite with the melt properties such as viscosity and surface tension. Both researches showed that the penetration would be enhanced by low viscosity and high surface tension. Okazaki *et al.*^[17] and Higuchi *et al.*^[18] also investigated the effect of the penetration length on the physical properties of the sinter. In the results obtained by both studies, the shatter index and tensile strength of the sinter were improved for the ores that were more penetrated by calcium ferrite. Lastly, Higuchi *et al.*^[18] also investigated how the phase formation of the assimilated area would be affected when several kinds of iron ores react with reagent-grade calcium ferrite. His results showed that the formation of desirable phases such as SFCA would be drastically affected depending on which type of ore is used.

The current study analyzed some high-temperature characteristics of several calcium ferrites which were prepared using different types of iron ores as the source of Fe₂O₃ sources. Therefore, the effect of iron ore type on the high-temperature properties of calcium ferrites was investigated. Finally, understanding the role of each iron ore in the high-temperature characteristics of calcium ferrite might provide the selection criteria for iron ores to be used in the sintering process. A new melt

index was adopted to precisely evaluate the calcium ferrites by figuring out their high-temperature characteristics. As the final objective of this study, the aforementioned calcium ferrites, with distinct high-temperature characteristics, were added to the sinter mix and had their effect on the sinter strength investigated.

II. EXPERIMENTAL

A. Materials Preparation

The current study used two kinds of iron ores which are commonly applied in the sinter plant of steelmaking companies. X-ray diffraction (XRD, CuK-alpha radiation, Bruker D8-Advance, Bruker, Massachusetts) analysis was conducted to identify the major phases present in each iron ore. As is shown in Figure 1, Ore A is a representative hematite-based iron ore (Fe₂O₃), while Ore B is a goethite-based ore (FeOOH). The chemical composition of both ores is shown in Table I. In addition, the chemical composition of a mix of ores composed of 50 wt pct Ore A and 50 wt pct Ore B was estimated by simple calculation in Table I. All the samples were analyzed by both wet chemical titration^[19] and inductively coupled plasma – atomic emission spectrometry (ICP-AES).^[20] As shown in Table I, the two iron ores used in the current study differ mostly in the content (wt pct) of T.Fe and SiO₂. Thus, Ore A is considered a higher-quality iron ore compared with Ore B. In addition, reagent-grade CaO (96 pct purity, SAMCHUN Chemical) was used. All the samples were crushed and sieved in a particle size below 250 μm.

The thermal characteristics of iron ores were analyzed in terms of TG-DSC (Thermogravimetric–Differential Scanning Calorimetry, TGA/DSC 1 Star system Mettler Toledo – Mettler Toledo AF, Schwerzenback, Switzerland). 100 mg of each iron ore was non-isothermally heated at a rate of 10 °C/min from room temperature to 1450 °C. Argon was constantly purged at 70 mL/min into the reactor. As shown in Figure 2, the difference in the dominant phases and chemical composition of the

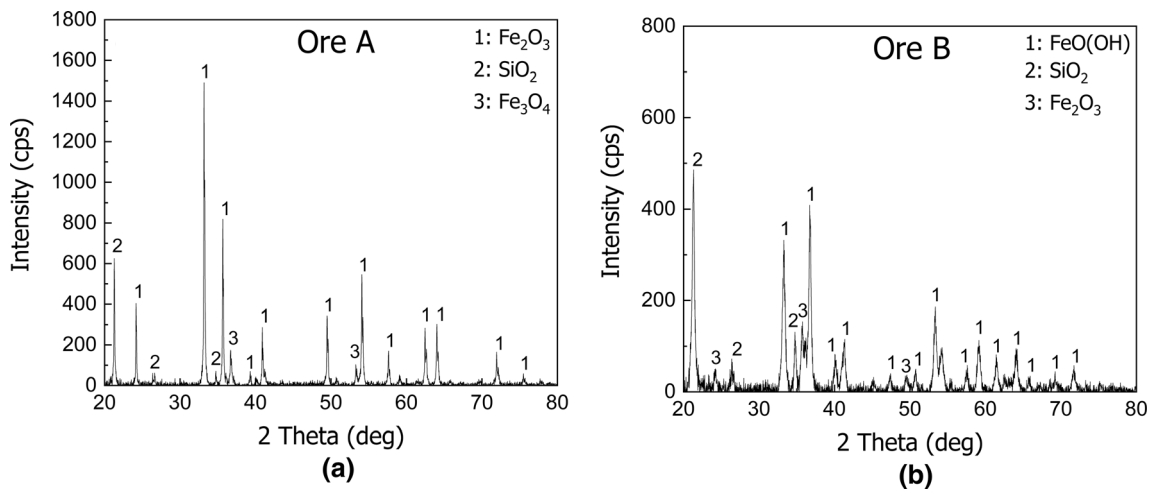


Fig. 1—Phase composition of iron ores identified by X-ray diffraction: (a) Ore A and (b) Ore B.

Table I. Chemical Composition of the Iron Ores Used (Weight Percent)

Iron Ores	T.Fe	FeO	M.Fe	Fe ³⁺	SiO ₂	Al ₂ O ₃	CaO	P ₂ O ₅	LOI
Ore A	65.20	0.46	0.07	64.77	1.52	1.25	0.07	0.15	2.70
Ore B	57.00	0.17	0.07	56.80	5.39	1.59	0.06	0.08	9.61
Mix of Ores	61.10	0.32	0.07	60.79	3.46	1.42	0.07	0.12	6.16

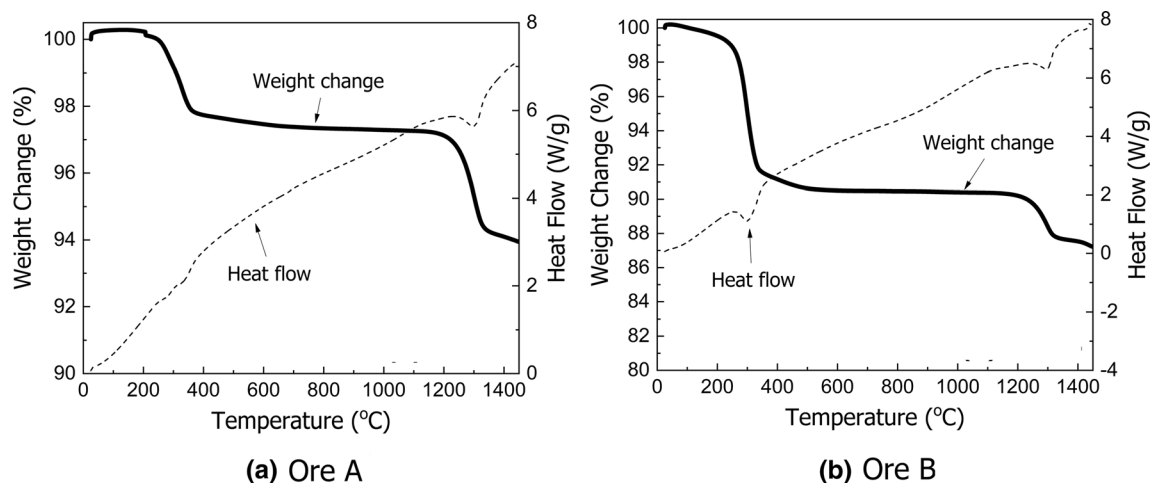


Fig. 2—Thermal feature of iron ores in terms of TG-DSC: (a) Ore A and (b) Ore B.

Table II. Added Amount of Reagent-Grade CaO to 100 g of Iron Ore (Grams)

Iron Ores	Fe ₂ O ₃	CaO
Ore A	94.55	34.60
Ore B	89.80	32.87
Mix of Ores	92.18	33.74

ores might be ascribed to the change in the behavior of Ore A and Ore B during heating. The iron ores showed significant weight loss in the similar temperature ranges of 200 °C to 400 °C and 1150 °C to 1300 °C. The losses in the low- and high-temperature region would be related to the dehydration and thermal decomposition of hematite, respectively.^[21] That is, Ore B showed the highest weight loss in the low-temperature region, while Ore A did in the high-temperature region. The major phase in Ore B is goethite in the form of hydroxide, which could release more water vapor than Ore A since Ore A contains more hematite than Ore B.

1. Calcium ferrites (CFs)

The calcium ferrite (CF) was prepared based on the CaO–Fe₂O₃ phase diagram presented by Phillips.^[22] Among the three well-known calcium ferrites; 2CF (2CaO·Fe₂O₃), CF (CaO·Fe₂O₃), and C2F (CaO·2-Fe₂O₃), Phillips^[22] reported that the one with the lowest melting point was achieved when the molar ratio between CaO and Fe₂O₃ is unity (weight ratio = 26 to 74). Based on this, three CFs were prepared using three kinds of iron ores; hematite-based Ore A, goethite-based Ore B, and a mix between the two ores as previously

presented in Table I. To achieve the molar ratio of 1 to 1 for forming CaO·Fe₂O₃ phase, the required amount of reagent-grade CaO was added to 100 g of each ore as shown in Table II. The amount of Fe₂O₃ was evaluated by X-ray fluorescence (XRF) analysis to guarantee the complete transformation of the goethite phase present in Ore B and Mix into hematite during the sample preparation.

After the required amount of reagent-grade CaO was added to each iron ore, the three mixes were heated to prepare the CFs. Firstly, the mixes were placed into an elevator furnace at 1400 °C for 5 minutes to guarantee the complete melting of the mixes. Then the melts were quenched in water and dried in an oven at 100 °C for 2 days. Finally, the samples were crushed and sieved in a particle size below 250 μm for further analyses. As shown in Figure 3, the XRD analysis confirmed the successful preparation of CFs whose major phase in the three CFs is CaO·Fe₂O₃.

2. Standard sinter mix (SSM)

The standard sinter mix was prepared in this study following the procedure of producing the sinter mix being used in steelmaking companies based on the fraction of iron ores present in the mix. Nowadays, the use of goethite-based iron ores is increasingly being used because of the depletion of high-grade hematite ores.^[12,15] Therefore, in the current study, 20 wt pct of Ore A and 80 wt pct of Ore B were first mixed, which amounts to 92 wt pct of the sinter mix. The remaining was occupied by reagent-grade CaO to keep the basicity level [(wt pct CaO)/(wt pct SiO₂)] at around 1.9 as shown in Table III. The standard sinter mix was

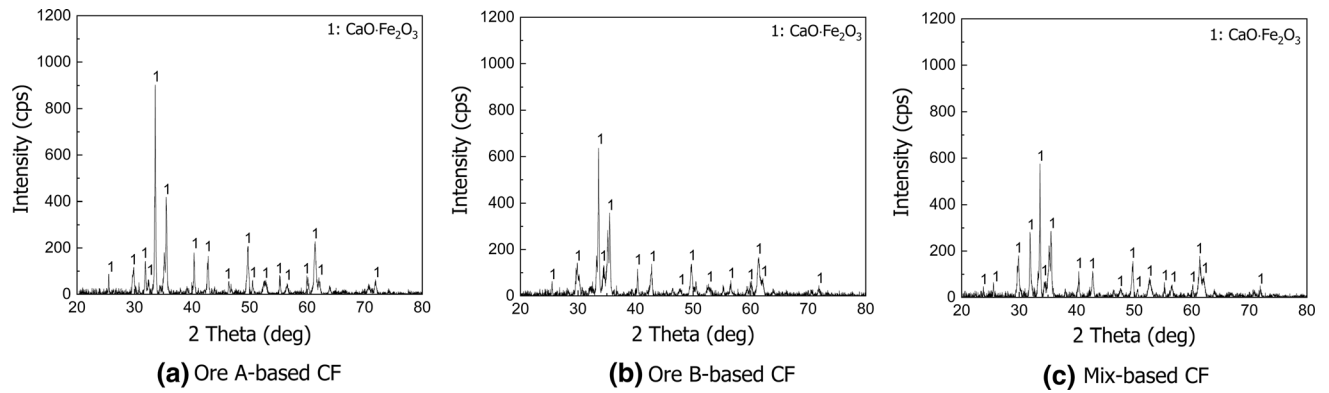


Fig. 3—Phase composition of CFs identified by X-ray diffraction: (a) Ore A-based, (b) Ore B-based and (c) Mix-based.

Table III. Chemical Composition of the Standard Sinter Mix (Weight Percent, db)

T.Fe	FeO	M.Fe	Fe ³⁺	SiO ₂	Al ₂ O ₃	CaO	P ₂ O ₅	Basicity (CaO/SiO ₂)
53.95	0.21	0.06	53.72	4.25	1.40	8.06	0.09	1.90

uniformly mixed for 3 hours employing the Turbula Mixer (T₂F Nr. 120,942 Switzerland) at 34 revolutions per minute.

B. Experimental Procedure

The objective of this study is to define an optimal condition for adding CFs to the sinter mix that maximizes the sinter strength. Firstly, the current research investigated several high-temperature characteristics of CFs such as melting behavior of CFs, fluidity of CFs, dissolution behavior of sinter mix into CFs, and penetration length of CFs into sinter mix. In addition to the experiments to evaluate the high-temperature characteristics of CFs, each CF was individually added to the standard sinter mix at different amounts and was subjected to compression testing to investigate the effect of adding CFs to the sinter mix on the sinter strength. The high-temperature characteristics of CFs might play an important role in the final sinter strength, as different binding mechanisms are expected to happen. Each experimental method was described in detail.

1. Melting behavior of CFs

The chemical composition of the iron ores used in this study to prepare the CFs is quite divergent in the levels of total Fe and SiO₂, which might affect the final composition of CFs and the melting behavior of CFs. To understand the thermal feature of each CF during heating, an alumina crucible (8 mm Diameter × 5 mm Height) containing 0.1 g of each sample was charged into the TG-DSC which was then non-isothermally heated at a rate of 10 °C/min from room temperature to 1450 °C in an Ar atmosphere of 70 mL/min.

2. Fluidity index (FI) of CFs

To clarify the effect of the iron ore source and consequent chemical composition on the fluidity of CFs, fluidity tests were carried out employing a lab-scale apparatus. About 0.8 g of CF was shaped into a cylindrical tablet employing a steel mold under a pressure of 20 MPa. Then, the disk was placed in an alumina crucible (65 mm Length × 20 mm Width × 10 mm Height). The crucible was charged into a gold-image furnace (VHT-E48, ULVAC-RIKO, Yokohama, Japan), tilted by an angle of about 30 degrees as represented in Figure 4. Air was constantly purged into the gold-image furnace during the total duration of the experiment. The heating pattern adopted in the current research followed the same conditions reported by Wu *et al.*^[11] The only difference was the target temperature. In this study, the temperature was set at 1300 °C, while Wu *et al.*^[11] performed the experiments at 1280 °C. In this study, the total gas flow rate used was adjusted to be 1 L/min. The fluidity of CFs was evaluated by comparing the vertical area of the CFs before and after the experiment as also shown in Figure 4. Finally, the fluidity index (FI) was calculated according to Eq. [1]^[11]

$$FI (-) = \frac{A_f - A_i}{A_i} \quad [1]$$

where A_f and A_i represent the area in cm² of CF before and after the fluidity test, respectively.

3. Dissolution of sinter mix into CFs

One of the important high-temperature characteristics to be investigated is how the standard sinter mix interacts with several CFs during heating. The interaction between the particles was evaluated in terms of

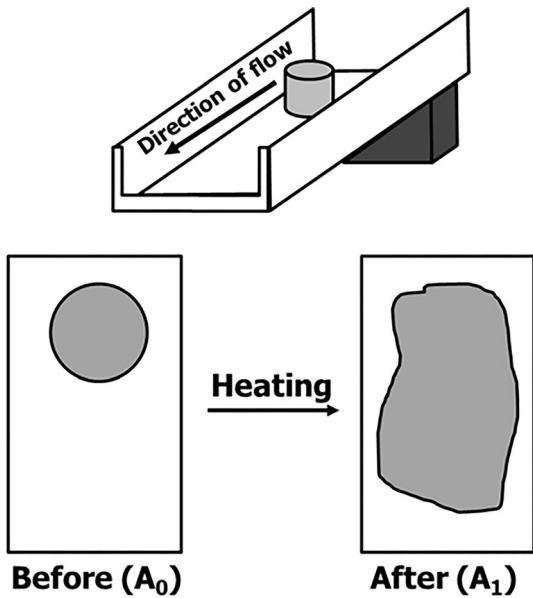


Fig. 4—Crucible arrangement inside the gold-image furnace for fluidity tests and vertical projected areas of CF before and after the experiment.

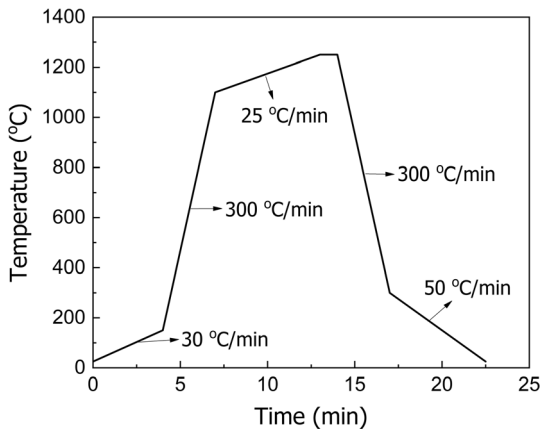


Fig. 5—Heating pattern applied to the dissolution behavior of sinter mix into CFs.

confocal scanning laser microscope (CSLM, Lasertec VL2000DX, Lasertec Corporation, Yokohama, Japan) and was employed to quantify the dissolved amount of sinter mix into CFs. Firstly, the CFs were pre-melted, cooled, and solidified inside the crucible, to coat and act as a substrate. After that, a standard sinter mix particle with a size of about $350 \mu\text{m}$ was placed over the CFs, in the middle of the crucible. This particle size was defined so the CSLM camera could always record the changes of the sinter mix particle. If the size was bigger than that, the recording screen would lose some parts of the particle. The samples were constantly exposed to an inert atmosphere (Argon) of 400 mL/min . Figure 5 represents the heating pattern adopted to evaluate the dissolution of sinter mix into CFs. Such a heating

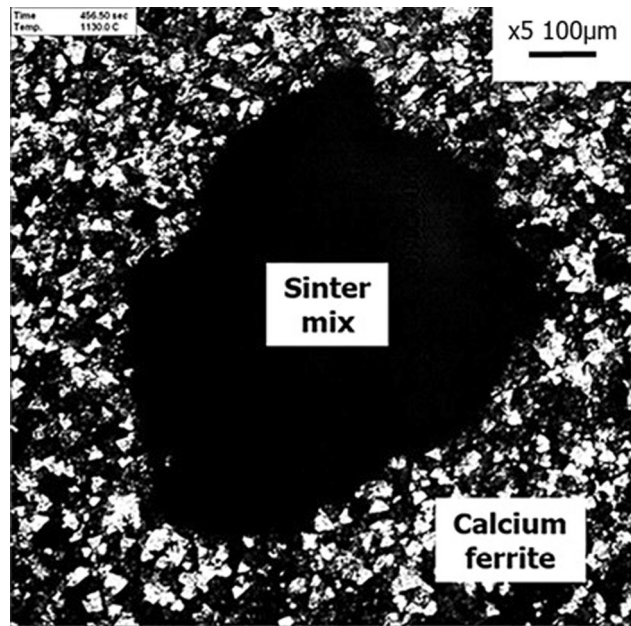


Fig. 6—Schematic representation of the area of sinter mix particle by CSLM.

pattern was defined as a rough estimation of the sintering process, which consists of a very high heating rate from room temperature to the ignition temperature, followed by a moderate heating rate until the target temperature. The dissolution behavior of the sinter mix particle was recorded from $1100 \text{ }^\circ\text{C}$ to $1250 \text{ }^\circ\text{C}$. The target temperature of $1250 \text{ }^\circ\text{C}$ was decided to understand the interaction between the CFs and the sinter mix particle in a low-temperature zone if compared to the temperatures reached during the sintering process. In addition, the mentioned target temperature is in the middle range of the melting temperature of CFs and the temperature of the fluidity index experiments.

To evaluate the amount of the sinter mix particle that actually dissolved into CFs, several screenshots were taken from the recorded video by CSLM at $1100 \text{ }^\circ\text{C}$, $1130 \text{ }^\circ\text{C}$, $1160 \text{ }^\circ\text{C}$, $1190 \text{ }^\circ\text{C}$, $1210 \text{ }^\circ\text{C}$, $1230 \text{ }^\circ\text{C}$, and $1250 \text{ }^\circ\text{C}$. In each temperature, the area of the sinter mix particle was estimated with the help of ImageJ software. By correlating the estimated area by the CSLM image with the area of a circle (πr^2), the radius of the sinter mix particle was evaluated at each temperature. Figure 6 represents one of the screenshots as an example to visualize how the area of the sinter mix particle was calculated. The sinter mix particle is represented by the black-painted particle shown in Figure 6. Based on this, the dissolution fraction of sinter mix into CFs can be evaluated by Eq. [2]:

$$\begin{aligned} \text{Dissolution fraction of sinter mix into CFs(pct)} \\ = \frac{r_i - r_f}{r_i} \times 100 \end{aligned} \quad [2]$$

where r_i and r_f represent the initial and final radius in μm of sinter mix and r_f , respectively.

4. Penetration length (L) of CFs into the sinter mix

To clarify the effect of iron ore source and its chemical composition on the penetration length of CFs into standard sinter mix, an assimilation test was carried out employing a lab-scale apparatus. Two samples were prepared for each experiment. About 0.3 g of CF and 1 g of sinter mix were shaped into cylindrical tablets with dimensions of 7 mm Diameter \times 1.5 mm Height and 10 mm Diameter \times 4 mm Height, respectively. The conditions to prepare the disk-shaped samples were the same as those applied for the fluidity tests. Then, the CF disk was placed over the sinter mix disk inside an alumina crucible (15 mm Diameter \times 10 mm Height). Figure 7 represents the layout of the samples and the projected penetration done by CF into the sinter mix. The crucible containing disks was put into the vertical tube furnace when the experimental temperature was achieved. Wu *et al.*^[11] reported that, depending on the temperature, three cases could have resulted from the two samples: un-assimilated, assimilated, or over-assimilated. Based on that, several tests were performed to determine the assimilation temperature for each system (CF + standard sinter mix). The samples were constantly exposed to an inert atmosphere (Argon) of 1 L/min. The system composed of CF and sinter mix was kept inside the vertical furnace at the desired temperature for 3 minutes. The mentioned holding time followed the one adopted by Park *et al.*^[5] to guarantee that sufficient reactions occur between the CFs and sinter mix. Finally, after the assimilation was finished, the cooled samples were mounted in resin and polished for further analyses such as optical microscope (OM, LEICA DM 4000 M, LEICA, Wetzlar, Germany), electron probe microanalysis (EPMA, JEOL JXA-8530F, JEOL Ltd., Tokyo, Japan), and energy-dispersive X-ray spectroscopy (EDS, JEOL JSM-7100F, JEOL Ltd., Tokyo, Japan). An optical microscope was employed to roughly quantify the penetration length of each CF into the sinter mix. EPMA was employed to refine the evaluation of penetration length of CFs based on the elemental distribution, especially calcium (Ca). EDS was employed to clarify the effect of CFs on the phase formation inside the assimilated region.

5. Compressive strength of sintered samples

To understand the effect of adding CF to the standard sinter mix on the bonding strength of final sinters, compression tests were conducted. Firstly, 2 and 5 wt pct of CFs were uniformly mixed with the standard sinter mix for 3 h employing the Turbula Mixer (T2F Nr. 120,942 Switzerland) at 34 revolutions per minute, to guarantee a homogeneous mix between the CFs and standard sinter mix. Then about 1 g of each sample was shaped into a cylindrical tablet (10 mm Diameter \times 4 mm Height). Seven samples were prepared: standard sinter mix (SSM), SSM containing 2 and 5 wt pct of Ore A-based CF, SSM containing 2 and 5 wt pct of Ore B-based CF, and SSM containing 2 and 5 wt pct of Mix-based CF. Before performing the compression tests, the samples were exposed to a reducing atmosphere to simulate the combustion of coal during the sintering process. This study used a similar gas mixture that was adopted by Hsieh *et al.*,^[23] a gas mixture composed of 75 vol pct Ar, 23 vol pct CO_2 , and 2 vol pct CO. The total gas flow rate was adjusted to be 1.5 L/min. Each sample was kept inside the furnace at 1250 $^\circ\text{C}$ for 3 minutes. Finally, after the samples were sintered, and cooled down to room temperature, the compression tests were conducted in an Instron MicroTester (MicroTester 5848, Instron, Massachusetts) at a loading rate of 10 mm/min. Several disks of each of the seven samples were analyzed, and the compressive strength of each sample was evaluated through the average value.

III. RESULTS

A. Melting Behavior of CFs

As the CFs were prepared from different iron sources—Ore A, Ore B and Mix, the melting behavior of CFs might be affected by the intrinsic properties of iron ores. That is why the CFs were exposed to temperatures around 1450 $^\circ\text{C}$ by TG-DSC. The thermal feature of CFs is shown in Figure 8. The heat flow patterns of CFs are almost identical among them except for the value of melting temperature. Pandey *et al.*^[24] conducted a similar experiment employing TG-DSC, but reagent-grade CF was used instead of iron ores as a source for the preparation of CFs in his research. Based on the results obtained by Pandey *et al.*,^[24] the melting

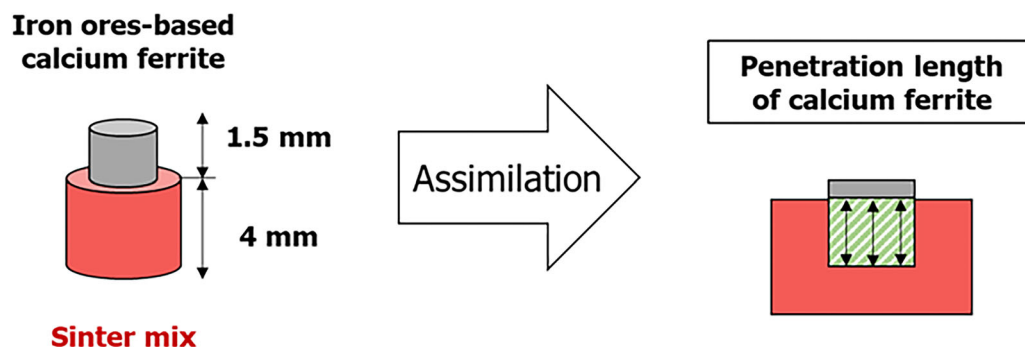


Fig. 7—Schematic of the samples system composed of CF and sinter mix tablets to measure the penetration length of melt.

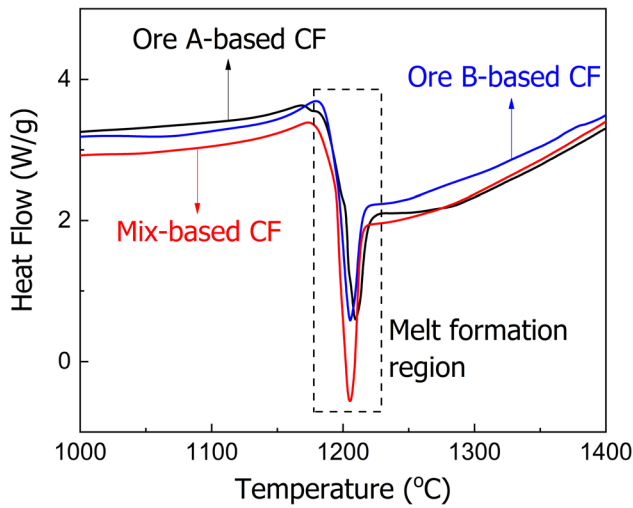


Fig. 8—Thermal feature of CFs in terms of TG-DSC.

Table IV. Amount of Gangue Oxides Present in CFs (Weight Percent)

CFs	SiO ₂	Al ₂ O ₃
Ore A-Based	1.13	0.93
Ore B-Based	4.06	1.20
Mix-Based	2.58	1.06

temperature of reagent-grade CF is around 1219 °C, while it was always below 1210 °C in this study. This discrepancy might be related to the diverse chemical composition of the samples, for example, the SiO₂ content, which might contribute to a decrease in the melting point of CFs.^[1,7,11]

As shown in Figure 8, Ore B-based CF has the lowest melting temperature of 1205 °C, followed by Mix-based (1206 °C) and Ore A-based (1209 °C). Even though the difference in the melting temperature is very small, it might be explained based on the highlighted discrepancy in the properties of iron ores. In this study, as the CFs were prepared from different iron ores, the amount of SiO₂ present in each CF should be different as shown by Table IV. Maeda *et al.*^[1] reported that the presence of 5 wt pct of SiO₂ in the reagent-grade CF decreased the necessary time to form CF and consequently increased the formation rate of CF compared with the sample without any addition of SiO₂. The results obtained in this study are in agreement with the one reported by Maeda *et al.*^[1] Ore B-based CF containing the highest amount of SiO₂ along the CFs used formed the melt faster than other CFs.

B. Fluidity Index (FI) of CFs

Fluidity could be considered to be one of the high-temperature properties of CF previously mentioned. The evaluation of FI is important to understand how the fluidity of CFs evolves since it is affected by different iron ores to prepare CFs. According to Oliveira *et al.*^[10] and Wu *et al.*,^[15] the fluidity of the liquid phase

might have an optimal value, which normally belongs to an intermediate level. Wu *et al.*^[11] similarly concluded his results. From his research, the bonding strength of the sinter was improved as the fluidity of the liquid phase increased. However, an increase in the fluidity might deteriorate the permeability of the sinter, that is, the productivity. Sukenaga *et al.*^[25] showed that the viscosity of calcium ferrite melt is inversely affected by the temperature. As shown in Figure 9(a), CF prepared from Ore A has the highest fluidity index, followed by Mix and Ore B. The obtained results are in good agreement with the prediction of viscosity in terms of FactSage 7.3, as presented in Figure 9(b). Ore A-based CF showed the smallest viscosity in the wide range of temperatures compared with Ore B and Mix-based CFs. The grade of the iron ore, that is, SiO₂ content, used to prepare each CF might result in the obtained results. In this study, the amount of added CaO to iron ore was fixed to form CaO·Fe₂O₃, which means that iron ores containing less gangue oxides, such as SiO₂ and Al₂O₃, will lead to the formation of a CF with higher fluidity. As shown in Figure 9(a), there is a linear relationship between the fluidity index of CFs and the SiO₂ and Al₂O₃ contents in CFs. Park *et al.*^[5] and Wu *et al.*^[16] obtained similar results to the current study. The CaO content was fixed during the sample preparation, which leads to higher fluidity indexes of the iron ores containing a fewer amount of gangue components. In contrast, Wu *et al.*^[15] fixed the basicity level of the sample mixture instead of the CaO content. Therefore, iron ores containing more SiO₂ in their composition required more CaO to keep the basicity constant, which enlarged the amount of low-melting-point compounds.

C. Dissolution Behavior of Sinter Mix Particle into CFs

Figure 10 shows the relationship between the dissolution fraction of the sinter mix particle and the experiment temperature for the three CFs used in this study. As previously explained, the dissolution fraction was evaluated according to Eq. [2] and represents how much the radius of the sinter mix particle was decreased during the heating. The mentioned reduction in the radius could be assumed to be the amount of dissolved sinter mix into the CF. The higher the dissolution fraction of the sinter mix particle, the better for the assimilation and the development of phases during the sintering process. The amount of sinter mix that actually dissolved into the CFs increased with increasing the temperature. The highest dissolution of sinter mix was obtained when Mix-based CF was used, while the lowest was the case of Ore A-based CF. Okazaki *et al.*^[17] concluded that the interaction between particles was improved in the presence of gangue components. This phenomenon might be the reason for the considerable gap between the dissolution of sinter mix into Mix- and Ore B-based CFs compared with Ore A-based. As shown in Table I, Ore A contains the lowest amount of gangue among the iron ores used. For the same reason, the amount of dissolved sinter mix was expected to be the highest when Ore B-based CF was used. However, Mix-based CF showed a higher interaction with the

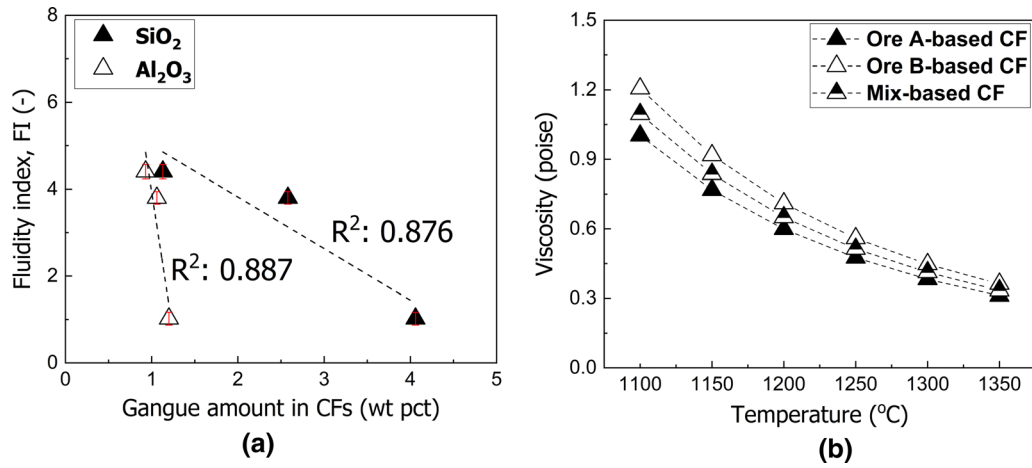


Fig. 9—Fluidity index of CFs: (a) Relationship with SiO₂ and Al₂O₃ contents present in CFs and (b) Prediction of viscosity in terms of FactSage 7.3.

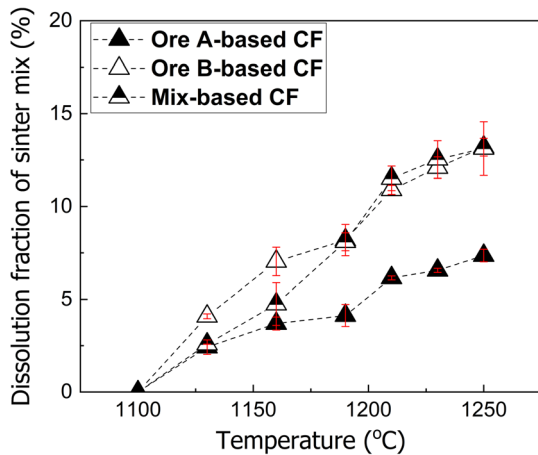


Fig. 10—Dissolution fraction of sinter mix particle into CFs with increasing the temperature.

sinter mix particle. In addition to the chemical composition of the CFs, another important factor that has a significant effect on the dissolution behavior of the sinter mix is the stirring speed of the particle that is being dissolved. Maeda *et al.*^[1] reported on their research that the rotation speed of hematite sample directly affects the dissolution of hematite into CF. As the speed increased, the dissolution amount was also increased. In this study, the sinter mix particle was not rotated during the experiment. However, the fluidity of CFs might encompass the effect of stirring reported by Maeda *et al.*^[1] As previously shown in Figure 9, the fluidity index of Mix-based CF is about 3.7 times greater than that shown by Ore B-based one, which might have contributed to the improved interaction between the sinter mix particle and the CF melt. That is why the results of Mix-based CF just became higher than that shown by Ore B-based above 1200 °C, as shown in Figure 10. The melting temperature of all CFs is between 1200 °C and 1210 °C. The contribution of the melt formation to the dissolution of sinter mix particles could be seen on the three curves. The slope between the data points at 1190

°C and 1210 °C is the highest for all CFs, which means that between those points, the CFs melted and enhanced the dissolution of sinter mix particle into the CFs.

D. Penetration Behavior of CFs into the Sinter Mix

The first step to quantify the penetration length of CFs is to guarantee that the two disks of CFs and sinter mix should be assimilated. The current study followed the method used by Wu *et al.*^[11] to find out if the assimilation was achieved or not. The system composed of CF and sinter mix was tested at 1200 °C, 1210 °C, and 1220 °C. At 1200 °C, the samples did not assimilate, whereas the CF could be easily removed from the top of the sinter mix disk. At 1220 °C, a temperature significantly higher than the melting point of all the CFs, the samples were over-assimilated, which means that the CF must spread too much over the surface of the sinter mix. Finally, the assimilation among all the CFs and sinter mixes was achieved at 1210 °C. For further analyses, the samples were cut in the lengthwise direction to expose the assimilated region. To complete the preparation procedure, the samples were also mounted and polished. Three samples were prepared; Ore A-, Ore B-, and Mix-based CFs assimilated with sinter mix. Figure 11 presents the penetration length in mm of each CF according to the visualization and average calculation through several optical microscope images of which a representative image of is represented in Figure 12. The penetrated fraction with reference to the height of the sinter mix tablet, which is 4 mm, is also plotted in Figure 11. The length penetrated by Ore A-based CF is the highest, followed by Mix- and Ore B-based CFs. To confirm the reliability of the optical microscopy images, EPMA mapping was carried out to quantify the penetration of CFs into the sinter mix. The method of evaluating the penetration length of melt into the sinter mix was based on the elemental distribution analyses of calcium (Ca) due to the significant difference in the level of Ca in the CF and sinter mix. CF contains about three times more CaO than the sinter mix, 26 and 8 wt pct, respectively. Figure 13 compares the elemental

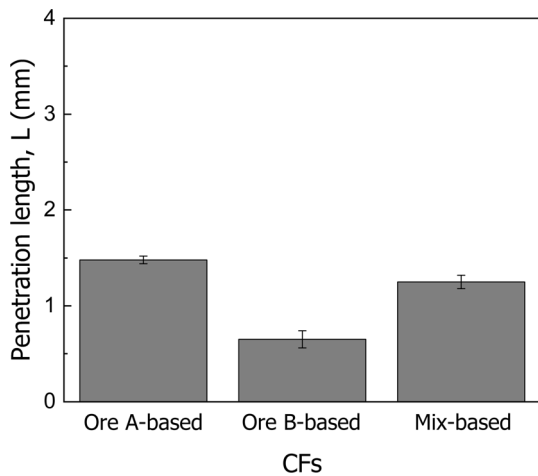
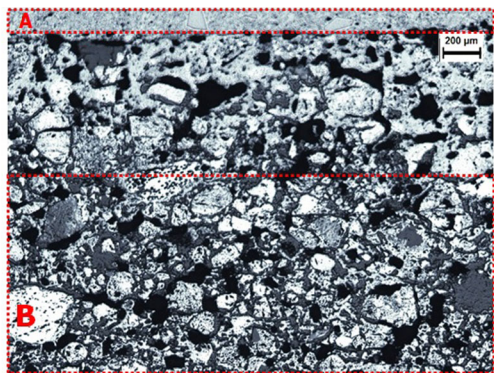


Fig. 11—Penetration length of CFs into sinter mix.



A: CF region / B: Sintered region / A-B: Assimilated region

Fig. 12—Microphotographical representation of penetration of Ore B-based CF into sinter mix by optical microscopy (OM).

distribution of Ca and Fe identified by EPMA mapping in the penetrated part of CF into the sinter mix. The assimilated region was highlighted by positioning dashed lines on the superior and inferior limits of the region. As represented in Figure 13, the penetration of Ore A-based CF is also the most, followed by Mix- and Ore B-based CFs. Despite the technique used, the ranking order of penetration length of CFs was kept constant.

As previously explained, three iron ores of different major phases and chemical compositions were used to prepare the CFs. The critical factor affecting the penetration behavior of CFs into the sinter mix might be the amount of gangue components present in the iron ores. Table V represents the content of SiO_2 and Al_2O_3 present in each CF. Ore A-based CF made from high-grade iron ore contains less amount of gangue compared with Ore B- and Mix-based CFs. The simultaneous effect of both SiO_2 and Al_2O_3 was defined as a combined effect and evaluated according to Eq. [3]. Figure 14 presents the correlation between the penetration length of CFs and gangue components. As the amount of both SiO_2 and Al_2O_3 in the ores increased, the penetration length achieved by CF significantly

deteriorated. When the penetration of CF was correlated to the combined effect of both gangue oxides simultaneously, the linear coefficient of the fitting was almost 1. The negative contribution of SiO_2 and Al_2O_3 on the penetration might be related to the change in the fluidity of CFs promoted by the presence of these oxides. The results obtained in the current research are in good agreement with previous studies. Several researches also correlated the penetration of CF with the chemical composition of iron ores.^[2,5,17,18] Okazaki *et al.*^[17] studied the effect of several components on the penetration of CF into the iron ore layer. It was found that the penetration length of CF is inversely proportional to the amount of SiO_2 , Al_2O_3 , and combined water present in the chemical composition of ores, while the effect of total Fe is very small. Nakashima *et al.*^[2] concluded that when SiO_2 and Al_2O_3 were added to reagent-grade CF ($\text{CaO}\cdot\text{Fe}_2\text{O}_3$), the penetration of melt deteriorated. Higuchi *et al.*^[18] and Park *et al.*^[5] conducted a similar experiment as Okazaki *et al.*,^[17] which also confirmed the negative influence of Al_2O_3 present in the iron ore composition on the penetration depth of reagent-grade CF. However, it is important to highlight that all the mentioned previous studies analyzed the interaction between reagent-grade CF and iron ores, while the current study used CFs and standard sinter mix, both prepared from real iron ores generally used in the steelmaking companies. This difference must be noticed because anyhow CF will be formed through the reaction between iron ores and limestone/lime during the sintering process. Therefore, the type of iron ore has great importance in the formation of CF.

$$\text{Combined effect} = [\text{wt pct SiO}_2] \times [\text{wt pct Al}_2\text{O}_3] \quad [3]$$

Identification and evaluation of the formed phases in the assimilated region might be one of the important tools to qualify the degree of interaction between CFs and sinter mix. The most desirable phase during the sintering process is known to be SFCA (silico-ferrite of calcium and aluminum),^[4,26] which could be considered to be a kind of CF,^[4,27] previously reported by Webster *et al.*^[4] as a Ca-rich ferrite containing silica and alumina. Several studies investigated the effect SiO_2 content on the phase's development of the sinter. It is important to highlight that the main difference between the iron ores used in this study is the SiO_2 content, as shown in Table I.^[28–31] Figure 15 represents the microphotographs of the assimilated regions obtained by scanning electron microscopy (SEM) where two images per CF system were analyzed. One represents the overview of the regions (Figures 15(a), (c), (e)) and the magnified ones to investigate the presence of SFCA-type phases or not inside the assimilated region (Figures 15(b), (d), (f)). Energy-dispersive X-ray spectroscopy (EDS) was employed to quantify the distribution of Fe, Ca, Si, Al, and O (at. pct). Table VI summarizes the elemental composition at different points of the assimilated region between CFs and sinter mix. Several points were analyzed for each CF system as shown in Figure 15. In addition to the major presence of the hematite phase, 'SFCA-related' phases are well distributed and formed

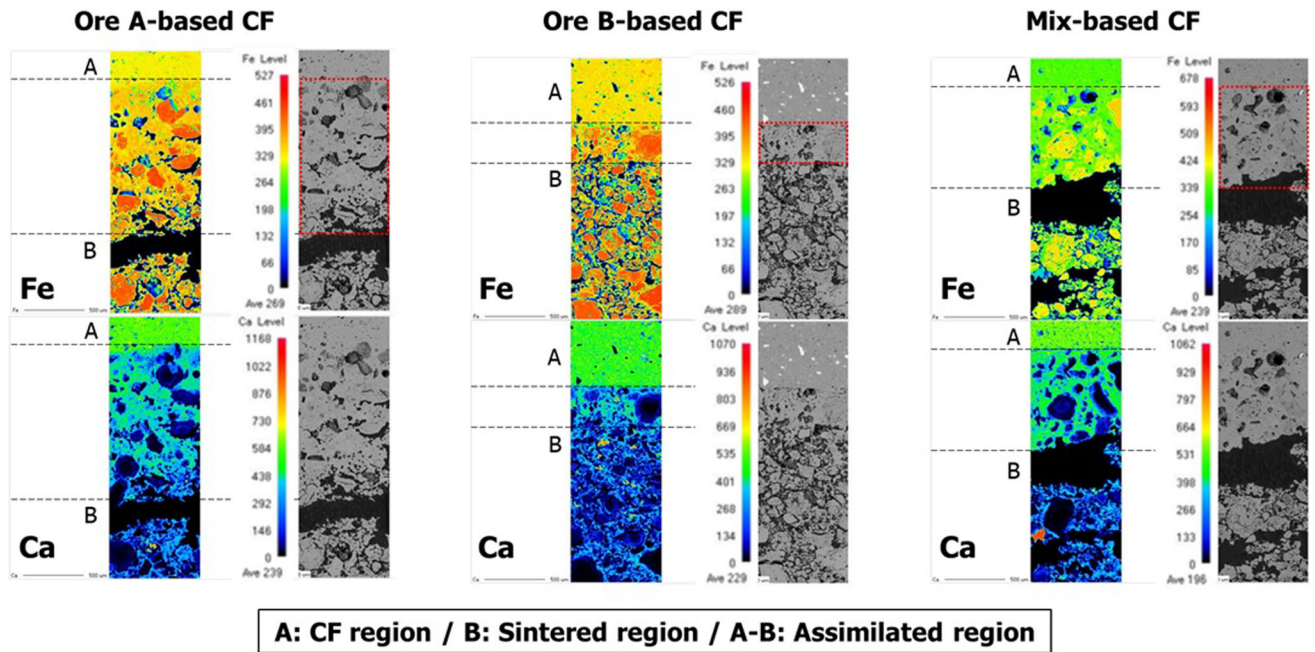


Fig. 13—Elemental distribution of Ca and Fe identified by EPMA mappings in the penetration of CFs into sinter mix. [$\times 40$].

Table V. Effect of Gangue Components Present in CF on the Penetration Length of Melt

CFs	SiO ₂ (Wt Pct)	Al ₂ O ₃ (Wt Pct)	Combined Effect	Penetration Length, L (mm)
Ore A-Based	1.13	0.93	1.05	1.48
Ore B-Based	4.06	1.20	4.87	0.65
Mix-Based	2.58	1.06	2.73	1.25

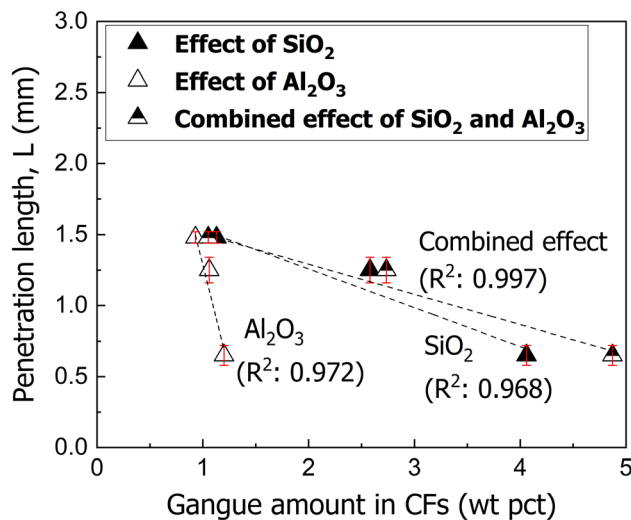


Fig. 14—Relationship between the penetration length of CFs into sinter mix and gangue amount in CFs.

inside the assimilated region of the three CFs with the sinter mix. Firstly, the CF melted and then penetrated into the sinter mix. During the penetration into the sinter mix, the CF melt reacted with the oxides

contained in the sinter mix. In both CF and sinter mix tablets, the main constituents are Fe₂O₃ and CaO. However, noticeable content of SiO₂ and Al₂O₃ is present in the sinter mix tablet. The dissolution of these two oxides into the CF melt was the driving force for the formation of ‘SFCA-related’ phases in the assimilated regions as shown in Table VI. The obtained results show that even though the CFs were prepared from different iron ore sources, containing different amounts of SiO₂, a similar bonding phase was formed. The reason for such a phenomenon might be related to the fixed composition of the sinter mix. Therefore, as the main constituents of the three CFs used in the current study, Fe₂O₃ and CaO were identical with a slight deviation in other components, the phase formation in the assimilated area was found to be similar. To corroborate the previous explanation, Higuchi *et al.*^[18] showed that the phase formation of the final sinter was mostly governed by the type of iron ore by adding a fixed level of CaO to several kinds of ores. They studied seven iron ores of different sources with diverse chemical compositions in the content of SiO₂, Al₂O₃, and combined water. However, the selection of iron ores for improving the formation of SFCA in the sinter would also affect the high-temperature characteristics of the CF formed during the sintering. As shown in this study, it is believed that the

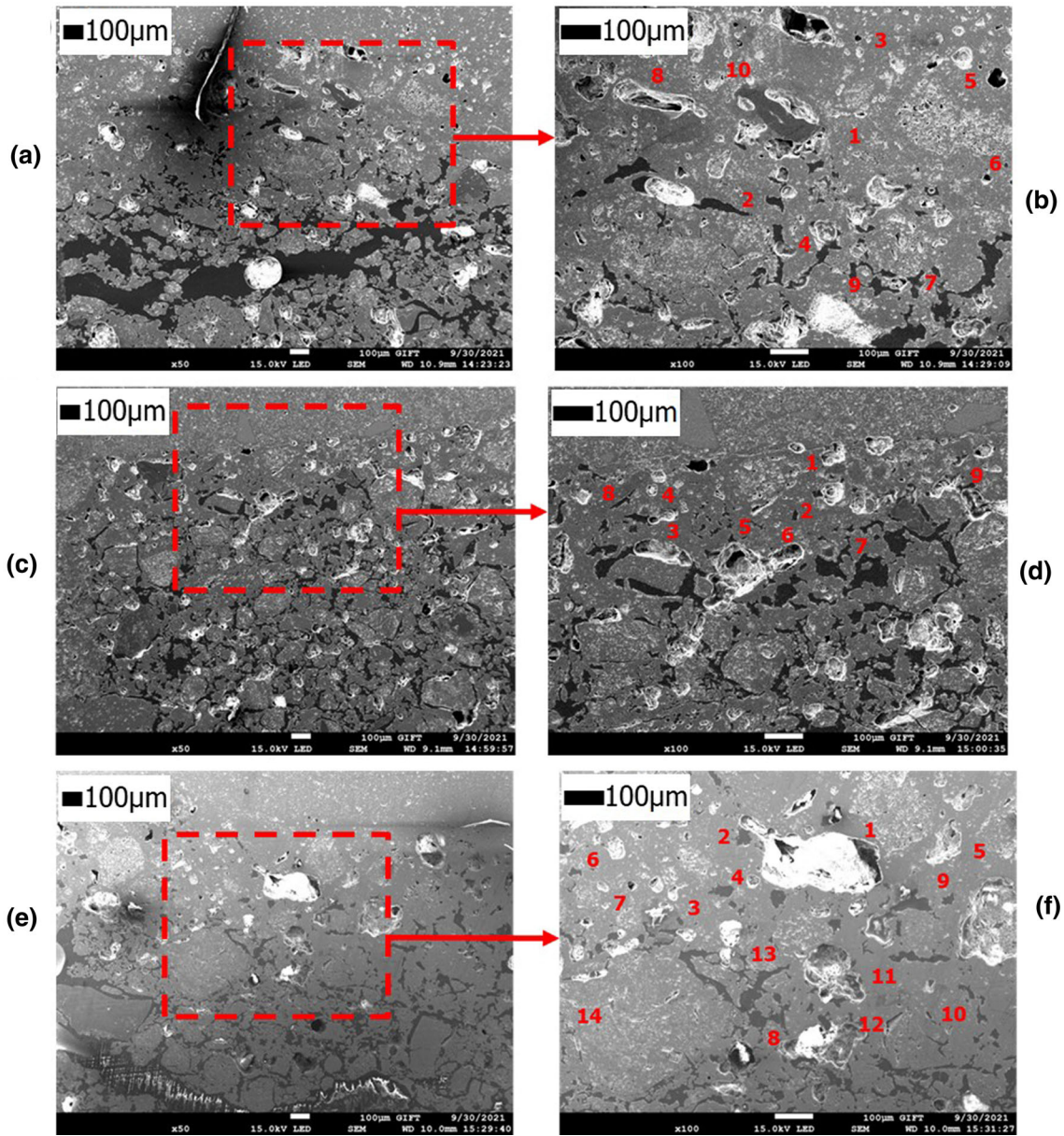


Fig. 15—Representation of the microstructures of the assimilated regions between calcium ferrites and sinter mix: (a), (b) Ore A-based CF, (c), (d) Ore B-based CF and (e), (f) Mix-based CF [(a), (c), (e): $\times 50$ /(b), (d), (f): $\times 100$].

presence of such gangue components in the CF might deteriorate the fluidity index of melt and consequently shorten the penetration length of this melt into the sinter mix, which might have adverse effects on the sinter quality. Okazaki *et al.*^[17] showed that iron ores more penetrated by reagent-grade CF had a better shatter index and product yield compared with less penetrated iron ores. Park *et al.*^[5] showed the same trend in view of product yield. That is the reason why ore blending is extremely required for the sintering process by balancing the properties of the ores in view of phase formation and high-temperature behavior, which will be decisive for the sinter quality.

IV. DISCUSSION

A. Derivation of Melt Index and Its Correlation with High-Temperature Characteristics of CFs

The high-temperature characteristics of CFs such as melting behavior, fluidity, dissolution amount of sinter mix, and penetration of CFs into sinter mix can be highly affected by the chemical composition of iron ores, especially by the level of SiO_2 and Al_2O_3 as shown in the previous sections and widely reported by other researchers^[2,5,17,18] Therefore, it might be important to derive a relationship among those characteristics of CFs for understanding their effects. German *et al.*^[32] discussed

Table VI. Elemental Composition in Assimilated Regions Between CFs and Sinter Mix by EDS Analyses

CFs	Points	Composition (Atomic Percent)				
		Fe	Ca	Si	Al	O
Ore A-Based	1	30.1	3.9	1.7	1.3	63.0
	2	26.7	9.0	1.9	1.2	61.2
	3	29.8	7.0	0.5	1.3	61.4
	4	27.9	8.4	1.9	1.0	60.8
	5	25.5	6.9	2.8	2.1	62.7
	6	26.5	7.6	2.6	1.6	61.7
	7	23.5	10.0	2.6	1.2	62.7
	8	27.5	8.4	1.6	1.2	61.3
	9	31.5	7.0	1.0	1.1	59.4
	10	30.5	6.1	0.9	0.9	61.6
Ore B-Based	1	31.6	7.0	1.3	1.1	59.0
	2	29.8	7.4	1.5	1.0	60.3
	3	25.0	7.4	3.0	1.7	62.9
	4	30.2	8.4	1.6	0.8	59.0
	5	28.2	6.9	2.7	1.6	60.6
	6	30.9	7.6	1.2	1.8	58.5
	7	28.8	8.4	1.7	0.7	60.4
	8	28.6	8.1	3.4	2.1	57.8
	9	32.3	7.0	0.8	0.6	59.3
Mix-Based	1	31.5	6.3	0.6	0.6	61.0
	2	30.4	7.7	1.4	0.8	59.7
	3	27.0	7.7	2.2	0.9	62.2
	4	26.0	6.9	3.0	2.0	62.1
	5	25.7	10.4	2.1	1.0	60.8
	6	31.2	8.4	1.4	0.9	58.1
	7	26.7	7.7	2.8	1.5	61.3
	8	26.3	6.2	2.6	1.1	63.8
	9	27.4	8.9	1.3	0.9	61.5
	10	21.7	7.1	4.7	0.9	65.6
	11	22.5	10.6	2.8	1.2	62.9
	12	28.2	7.0	2.2	1.2	61.4
	13	30.7	4.7	1.3	0.8	62.5

Table VII. Evaluated Melt Indices of the Three CFs

CFs	MI	MI (SiO ₂)	MI (Al ₂ O ₃)	Penetration Length, L ² (mm ²)
Ore A-Based	0.70	0.62	0.75	2.19
Ore B-Based	0.10	0.02	0.08	0.42
Mix-Based	0.31	0.12	0.29	1.56

the phenomenon of interacting systems during liquid formation in general. His research stated that the penetration rate of the liquid into the solid–solid interfaces was dependent on the reactivity of the liquid, its viscosity, and the contact angle. Based on the mentioned factors, the depth of liquid penetration L_L could be estimated according to Eq. [4].^[32] Higuchi *et al.*^[18] adopted the same equation in their study:

$$L_L^2(m) = \frac{d_P \gamma_{LV} t \cos \theta}{4\eta} \quad [4]$$

where d_P (m) is the diameter of the capillary tube, γ_{LV} (J/m²) is the surface energy between melt and vapor, t (s) is the time, θ (°) is the contact angle between melt and solid, and η (Pa s) is the viscosity of the melt. Therefore, the reactivity of the liquid mentioned by German *et al.*^[31] might be related to the terms d_P , γ_{LV} , and t because θ and η are well defined as contact angle and viscosity, respectively.

Similarly, the current study correlated the penetration length of CFs with the chemical (reactivity) and physical (viscosity) properties of the melt. Based on the characteristics of CFs investigated in this research, the dissolution fraction of sinter mix into CFs might represent the reactivity of melt, and the fluidity index represents the viscosity. A melt index (MI) was derived to simply reflect the characteristics of CFs, as represented by Eq. [5]. According to Eq. [5], the melt index could be increased by the fluidity index of CFs and decreased by the dissolution amount of sinter mix into CFs. This relationship is similar to the one represented in Eq. [4]. Fluidity and viscosity are inversely correlated, while the wettability of the melt is increased by decreasing the contact angle and increasing the concentration of solid particles dissolved in the melt, which might deteriorate the penetration length of the melt.

$$\begin{aligned} \text{Melt index, MI (-)} \\ = \frac{\text{Fluidity index of CFs (FI)}}{\text{Dissolution fraction of sinter mix into CFs}} \quad [5] \end{aligned}$$

Table VII summarized the evaluated melt indices (MI) of the three calcium ferrites. MI (SiO₂) and MI (Al₂O₃) represent the effect of the content of SiO₂ and Al₂O₃ in the CFs on the melt index, respectively. That is, the values presented in Table VII for MI (SiO₂) and MI (Al₂O₃) were obtained by dividing the values in MI with the content of SiO₂ or Al₂O₃ shown in Table V. Such adjustment was proposed to confirm whether the effect of the aforementioned gangue oxides already contributed when the high-temperature characteristics were considered to derive the melt index (MI) or not. Figure 16 summarizes the relationship between the square of penetration length and melt indices. The penetration length of CFs has a positive correlation with the melt index, which means that the penetration length is the highest when related to a melt with high fluidity index and a low dissolved amount of sinter mix. A similar trend was found by Nakashima *et al.*^[2] and Higuchi *et al.*^[18] In both researches, the square of penetration length of reagent-grade CF into iron ores was increased when the ratio of surface tension to viscosity (γ/η) was also increased. In Figure 16, the linearity of the relationship between the square of penetration length and MI was evaluated to be 0.863 (R^2). However, in case the melt indices were corrected by the content of SiO₂ and Al₂O₃, the linearity deteriorated to 0.706 for MI (SiO₂) and 0.833 for MI (Al₂O₃). This might be ascribed to the influence of the gangue components already existing in the CFs on the fluidity index and dissolution ratio.

B. Effect of Adding CFs to the Standard Sinter Mix (SSM) on the Compressive Strength of Sinter and Its Correlation with the Derived Melt Indices

The compressive strength of the sinters prepared from the standard sinter mix containing two levels of CFs is shown in Figure 17(a) with respect to that from the standard sinter mix. The addition of CF to the sinter mix improved the sinter strength compared with the sinter not containing CF. This might be related to the low melting temperature of the CFs as shown in Figure 8. The sintering at 1250 °C for 3 min resulted in the formation of a complete melt of CF inside the sample, which promoted higher bonding due to the formation of the liquid phase. A similar finding was obtained by previous studies.^[33,34] Wang *et al.*^[33] investigated the effect of adding carbide slag (CS) on the sinter properties. As the carbide slag was mainly composed of $\text{Ca}(\text{OH})_2$, the addition of CS improved

the solid-phase reaction due to the presence of more bonding phase and, consequently, improved the sinter cold strength. In the case of Dishwar *et al.*,^[34] the increase in the basicity level of pellets hardened at 1200 °C improved the crushing strength of the samples, mainly because the porosity was decreased by the higher binding ability of liquid phase. However, the results shown in Figure 17(a) indicate that the compressive strength of the sinter added by CFs might be affected by the type and amount of CFs. As the amount of CF in the sinter mix increases from 2 to 5 wt pct, the compressive strength of the sinter showed different behavior depending on which calcium ferrite is added. Such phenomena might be ascribed to the melt index of the sinter mix composed of standard sinter mix and CF, which was exposed to high temperatures. When adding 5 wt pct of CF to standard sinter mix, Ore A-based CF of high melt index might have flown to the bottom of the sample leaving some pores on the upper part of the sample, which might have contributed to decreasing the compressive strength of the sinter compared with 2 wt pct addition. Wu *et al.*^[15] derived a relationship between the sinter strength and fluidity index of ore blends. In his results, there was a peak that represented the optimum value of fluidity that improved the shatter index of the sinter. He also found that a further increase in the fluidity level of ore blends would deteriorate the sinter strength due to the generation of large pores on the upper part of the sinter. In the current study, the bonding mechanism of Ore B- and Mix-based CFs at 5 wt pct appears to be similar. Compared with Ore A-based CF, the lower melt index allowed the liquid phase to bind more particles without flowing down the bottom of the sample; simply the calcium ferrite filled the spaces between the solid particles. Therefore, as shown in Figure 17(b), when the adding amount of CF was fixed at 2 wt pct, the compressive sinter strength has a linear relationship with the derived melt index where the linear coefficient was equal to 0.935. Consequently, from the relationship between the penetration length of

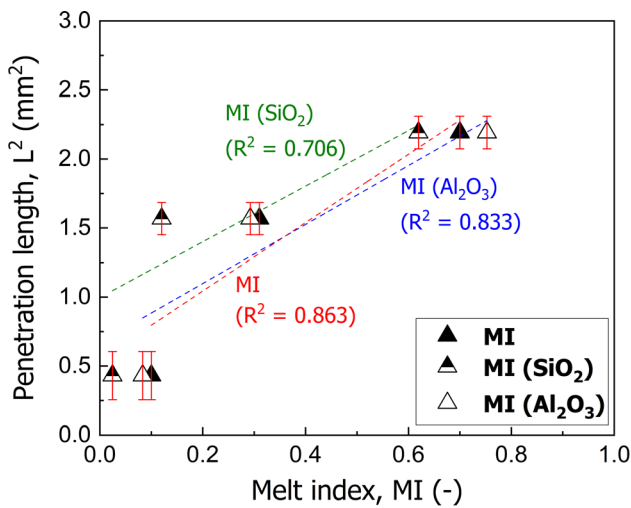


Fig. 16—Relationship between penetration length of CFs and their melt indices.

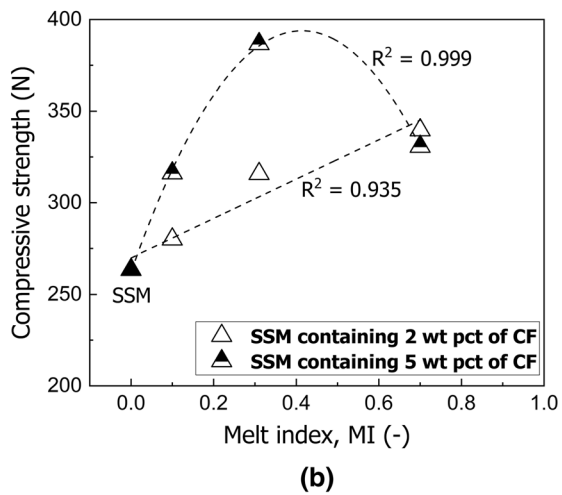
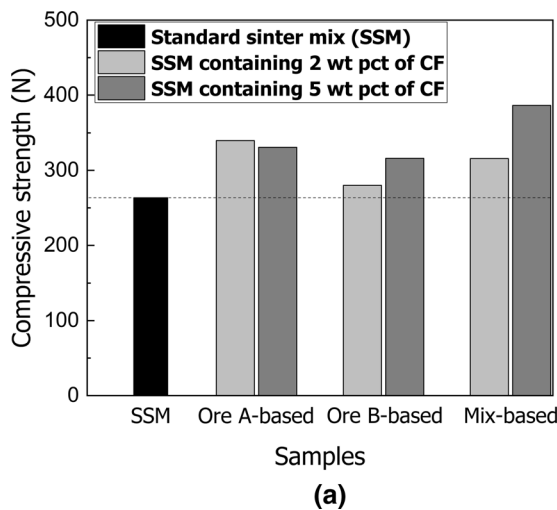


Fig. 17—Compressive strength of sintered samples: (a) Effect of additional amount of CF and (b) Relationship between the compressive strength and the melt index.

CFs and melt index shown in Figure 16, it could be concluded that the compressive strength is also directly related to the penetration length of CFs into sinter mix, which increased in the case of CFs with high penetration length. However, as shown in Figure 17(b), the linear relationship between the compressive strength and melt index at 2 wt pct addition of CF was corrected into a second-order polynomial at 5 wt pct addition, which has a fitting coefficient equals to 0.999. The polynomial fitting found by the current study is very similar to the one reported by Wu *et al.*^[15] Thus, for improving the sinter strength by adding CFs, the adding level of CF might be an important parameter since CFs are made from different sources of iron ores. Summarizing it, CFs with high melt index will maximize the sinter strength at small levels—Ore A-based CF at 2 wt pct, while CFs with low melt index at the high adding amount—Ore B- and Mix-based CFs were improved up to 5 wt pct. Among the CFs and adding levels investigated in this study, the use of Mix-based CF achieved higher strength compared with the other CFs, which might be related to the combination of characteristics of both Ore A- and Ore B-based CFs.

C. Mechanism of Adding CFs Prepared from Several Iron Ores Containing Different Gangue Amount to the Standard Sinter Mix

Figure 18 summarizes the suggested mechanism to explain the effect of the chemical composition of raw iron ores used to prepare several CFs on the formation of sinter. Firstly, consider the use of Ore A which contains a low amount of gangue to prepare the CF. The melt phase of the Ore A-based CF will have a big contact angle with the solid particles, *e.g.*, the standard sinter mix. The large contact angle means high surface tension, which would end up with the decrease in the dissolved amount of sinter mix particles into the CF.^[32]

To corroborate such a sentence, Nakashima *et al.*^[2] showed that the addition of both SiO₂ and Al₂O₃ to a reagent-grade CF decreased the contact angle at a fixed time, which led to a high spreading rate over the substrate and a small penetration length of CF into the substrate. Thus, as the standard sinter mix particles did not dissolve into the CFs, the fluidity of the CFs will not be significantly affected by the presence of new gangue components in the melt and will be able to penetrate more deeply through the sinter mix.^[17] In the case of using iron ores containing a high amount of gangue (Ore B), the mechanism could be exactly the opposite of the one shown by Ore A-based CF, as represented in Figure 18. The increase in the penetration length and high melt index will consequently lead to higher bonding between the particles and improvement of strength.^[18] The difference in how the CFs affect the sinter strength is summarized in Figure 18. CFs containing a small amount of gangue will improve the strength up to a certain level of addition. When the amount of Ore A-based CF was increased inside the sinter mix, more amount of melt would flow to the lower and bottom sections of the sample, resulting in the segregation of melt. Wu *et al.*^[15] reported a similar conclusion by mentioning that the shatter index of the sinter was improved up to a certain level of fluidity, which was then followed by deterioration. In contrast, CFs containing a high amount of gangue would improve the sinter strength as the amount of CF inside the sinter mix increased. The amount of liquid phase will increase, and simultaneously, due to the poor fluidity, there will be no melt found in the bottom section, which will finally improve the sinter strength. Another possibility for the increase in the sinter strength up to a certain additional level of Ore A-based CF might be related to the development of pores. As the fluid liquid phase spreads through more area inside the sample, this phase might act as a nucleation site for finer pores,^[32] which would

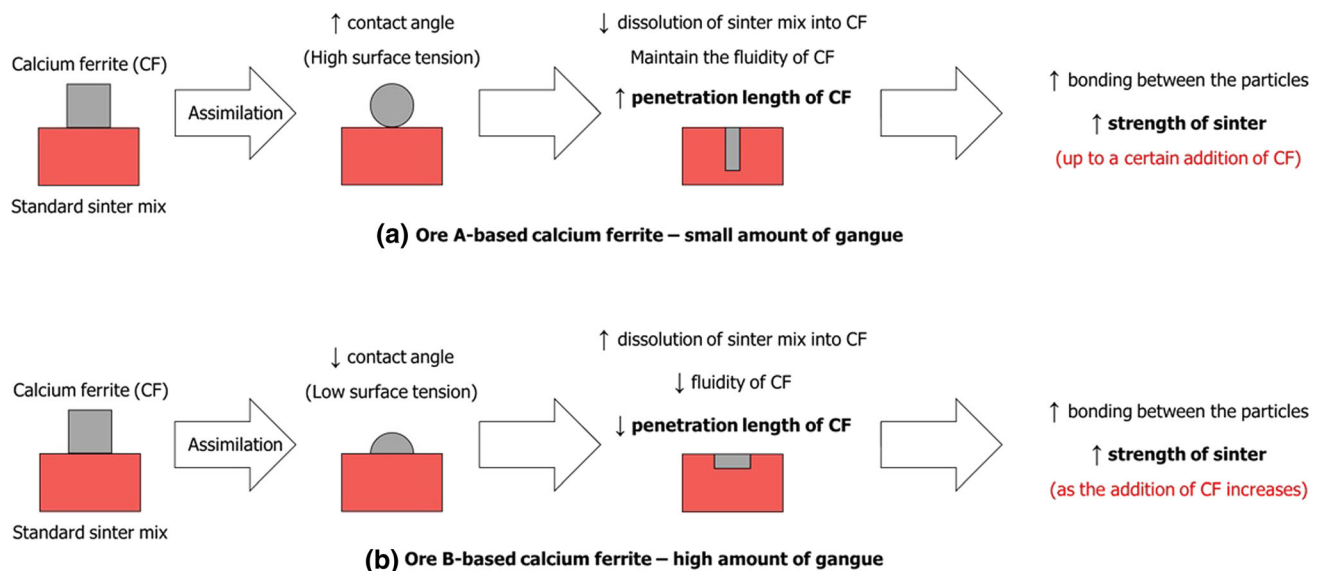


Fig. 18—Schematic mechanism of the effect of gangue amount present in raw iron on sinter strength when adding CFs to the standard sinter mix: (a) Ore A-based calcium ferrite and (b) Ore B-based calcium ferrite.

contribute to an improvement in the sinter strength.^[11] This phenomenon would happen to Ore B-based CF in case the additional amount is higher than that used for Ore A-based CF, as the fluidity of the liquid phase provided by Ore B-based CF is much lower and it would affect the ability of the melt to spread inside the sample.

V. CONCLUSIONS

It was studied how the CFs prepared from a different source of iron ores affected the high-temperature characteristics such as melting behavior, fluidity index, dissolution behavior of sinter mix particle into CF, and penetration length of CF. From the findings, the following conclusions were obtained.

1. The CFs prepared from several iron ores showed a variety of high-temperature characteristics. The diverse chemical composition of the ores might have resulted in such a difference. For example, Ore B contains a significantly higher level of SiO₂ than Ore A. The presence of gangue components in Ore B might have contributed to the decrease in the melting point of the Ore B-based CF, the fluidity index and the penetration length into the sinter mix. The gangue components also increased the dissolution of the sinter mix into CFs.
2. The penetration length of CFs was directly affected by the amount of gangue components in the CFs, especially by Al₂O₃ compared with SiO₂. The linearity (R^2 value) of the relationship between penetration length and content of Al₂O₃ present in CFs was calculated to be 0.972, while the case of SiO₂ was 0.968. Considering the combined effect of both oxides, the linearity was evaluated to be 1, which indicated the great importance of gangue components.
3. The phases formed in the assimilated region between CF and sinter mix were drastically not affected by changing the CF used. In all the cases, SFCA-related phases were identified. Such a phenomenon might confirm that the sinter mix played the main role in the phase formation by the assimilation reaction, which might be related to the amount of gangue components that dissolved into the CF melt.
4. A melt index was derived to evaluate the high-temperature characteristics of CFs in terms of the ratio of the fluidity index of CFs to the dissolution ratio of sinter mix into CFs. It was found that the melt index could be positively correlated with the penetration length, which indicates that CF with high fluidity and low dissolved amount of sinter mix would represent high penetration into the sinter mix.
5. The compressive strength of the standard sinter was improved when adding CFs at different levels. In the case of adding 2 wt pct, the compressive strength had a linear relationship with the derived melt index, which indicates that CFs with high fluidity index and low dissolution ratio could enhance the sinter strength. CFs with a high melt index would improve the sinter strength at small levels, while CFs with a low melt index increase it at high amounts.

6. The effects of adding CF to the standard sinter mix might be explained as follows: firstly, the selection of a specific iron ore to prepare the CF would have a great influence on the interaction between CF and sinter mix. Ores containing a low amount of gangue components would produce a CF whose melt has a large contact angle with the sinter mix, which would lead to high surface tension. This would consequently decrease the dissolution fraction of the sinter mix into the CF. With a low dissolved amount of sinter mix in the CF, the fluidity index of CF would not be greatly changed, which might result in an increase in the penetration length. That is, the addition of CFs would finally improve the sinter strength, but the proper level of CF added might differ according to the type of iron ores used.

CONFLICT OF INTEREST

On behalf of all authors, the corresponding author states that there is no conflict of interest.

REFERENCES

1. T. Maeda, K. Nishioka, K. Nakashima, and M. Shimizu: *ISIJ Int.*, 2004, vol. 44(12), pp. 2046–51.
2. K. Nakashima, N. Saito, S. Shinozaki, R. Tanaka, T. Maeda, M. Shimizu, and K. Mori: *ISIJ Int.*, 2004, vol. 44(12), pp. 2052–56.
3. S. Wu, D. Oliveira, Y. Dai, J. Xu, and H. Chen: *Adv. Mater. Res.*, 2011, vol. 201–203, pp. 1780–86.
4. N.A.S. Webster, M.I. Pownceby, I.C. Madsen, and J.A. Kimpton: *Metall. Mater. Trans. B*, 2012, vol. 43B, pp. 1344–57.
5. T.J. Park, B.C. Kim, and I. Sohn: *Steel Res. Int.*, 2021, vol. 92(2100206), pp. 1–7.
6. S. Yoshimura, K. Kurosawa, Y. Gonda, S. Sukenaga, N. Saito, and K. Nakashima: *ISIJ Int.*, 2009, vol. 49(5), pp. 687–92.
7. X. Ding and X. Guo: *Metall. Mater. Trans. B*, 2015, vol. 46B, pp. 1742–50.
8. X. Jiang, J. Zhao, L. Wang, H. An, Q. Gao, H. Zheng, and F. Shen: *ISIJ Int.*, 2021, vol. 61(1), pp. 86–92.
9. H. Noda, H. Yanaka, R. Yamamoto, H. Kawata, and Y. Yamaoka: *Trans. ISIJ*, 1985, vol. 25(11), pp. 1103–10.
10. D. Oliveira, S. Wu, Y. Dai, J. Xu, and H. Chen: *J. Iron Steel Res. Int.*, 2012, vol. 19(6), pp. 1–5.
11. S. Wu, G. Zhang, S. Chen, and B. Su: *ISIJ Int.*, 2014, vol. 54(3), pp. 582–88.
12. R. Mezibricky, M. Frohlichova, R. Findorak, and V. Sue Goettgens: *Minerals*, 2019, vol. 9(2), pp. 128–52.
13. S. Wu, H. Han, H. Li, J. Xu, S. Yang, and X. Liu: *Int. J. Miner. Metall. Mater.*, 2010, vol. 17(1), pp. 11–16.
14. D. Fernandez-Gonzalez, I. Ruiz-Bustinza, J. Mochon, C. Gonzalez-Gasca, and L.F. Verdeja: *Miner. Process. Extr. Metall. Rev.*, 2017, vol. 38(4), pp. 254–64.
15. S. Wu and X. Zhai: *Metall. Res. Technol.*, 2018, vol. 115, pp. 505–20.
16. S. Wu, H. Li, W. Zhang, and B. Su: *Metals*, 2019, vol. 9(4), pp. 404–16.
17. J. Okazaki, K. Higuchi, Y. Hosotani, and K. Shinagawa: *ISIJ Int.*, 2003, vol. 43(9), pp. 1384–92.
18. K. Higuchi, J. Okazaki, and S. Nomura: *ISIJ Int.*, 2020, vol. 60(4), pp. 674–81.
19. Japan Industrial Standard (JIS): *Iron ores – Method for determination of acid soluble iron (II) content* (JIS Standard No. M8213:1995).
20. International Organization for Standardization (ISO): *Iron ores – Determination of various elements – Inductively coupled plasma atomic emission spectrometric method* (ISO Standard No. 11535:2006).

21. Y. Qu, Y. Yang, Z. Zou, C. Zeilstra, K. Meijer, and R. Boom: *ISIJ Int.*, 2014, vol. 54(10), pp. 2196–205.
22. B. Phillips and A. Muan: *J. Am. Ceram. Soc.*, 1958, vol. 41(11), pp. 445–54.
23. L. Hsieh and J.A. Whiteman: *ISIJ Int.*, 1989, vol. 29(1), pp. 24–32.
24. V.K. Pandey, R.K. Duchaniya, U. Pandel, and S. Yadav: *AIP Conf. Proc.*, 2019, vol. 2148(030014), pp. 1–6.
25. S. Sukenaga, K. Ohara, H. Yamada, T. Wakihara, and H. Shibata: *Metall. Mater. Trans. B*, 2021, vol. 52B, pp. 1945–49.
26. N.V.Y. Scarlett, M.I. Pownceby, I.C. Madsen, and A.N. Christensen: *Metall. Mater. Trans. B*, 2004, vol. 35B, pp. 929–36.
27. S. Nicol, J. Chen, M.I. Pownceby, and N.A.S. Webster: *ISIJ Int.*, 2018, vol. 58(12), pp. 2157–72.
28. W. Wang, D. Yang, Z. Ou-yang, R. Xu, and M. Song: *Metall. Mater. Trans. B*, 2019, vol. 50B, pp. 678–87.
29. S. Nicol, E. Jak, and P.C. Hayes: *Metall. Mater. Trans. B*, 2019, vol. 50B, pp. 2706–22.
30. S. Nicol, E. Jak, and P.C. Hayes: *Metall. Mater. Trans. B*, 2019, vol. 50, pp. 3027–38.
31. R.F. Xin and X.M. Guo: *Metall. Mater. Trans. B*, 2022, vol. 53B, pp. 1904–19.
32. R.M. German, P. Suri, and S.J. Park: *J. Mater. Sci.*, 2009, vol. 44, pp. 1–39.
33. G. Wang, J. Zhang, Z. Liu, Y. Wang, Y. Li, and B. Zhang: *Metall. Mater. Trans. B*, 2022, <https://doi.org/10.1007/s11663-022-02514-5>.
34. R.K. Dishwar, A.K. Mandal, and O.P. Sinha: *Metall. Mater. Trans. B*, 2019, vol. 50B, pp. 617–21.

Publisher's Note Springer Nature remains neutral with regard to jurisdictional claims in published maps and institutional affiliations.

Springer Nature or its licensor holds exclusive rights to this article under a publishing agreement with the author(s) or other rightsholder(s); author self-archiving of the accepted manuscript version of this article is solely governed by the terms of such publishing agreement and applicable law.